We are IntechOpen, the world's leading publisher of Open Access books Built by scientists, for scientists

4,800
Open access books available

122,000
International authors and editors

135M
Downloads

Our authors are among the

154
Countries delivered to

TOP 1%
most cited scientists

12.2%
Contributors from top 500 universities

CLARIVATE ANALYTICS BOOK CITATION INDEX INDEXED

WEB OF SCIENCE™

Selection of our books indexed in the Book Citation Index in Web of Science™ Core Collection (BKCI)

Interested in publishing with us?
Contact book.department@intechopen.com

Numbers displayed above are based on latest data collected.
For more information visit www.intechopen.com

Chapter 12

Simulation of Morphological Effects on Thermoelectric Power, Thermal and Electrical Conductivity in Multi-Phase Thermoelectric Materials

Yaniv Gelbstein

Additional information is available at the end of the chapter

http://dx.doi.org/10.5772/65099

Abstract

Multi-phase thermoelectric materials are mainly investigated these days due to their potential of lattice thermal conductivity reduction by scattering of phonons at interfaces of the involved phases, leading to the enhancement of expected thermoelectric efficiency. On the other hand, electronic effects of the involved phases on thermoelectric performance are not always being considered, while developing new multi-phase thermoelectric materials. In this chapter, electronic effects resulting from controlling the phase distribution and morphology alignment in multi-phase composite materials is carefully described using the general effective media (GEM) method and analytic approaches. It is shown that taking into account the specific thermoelectric properties of the involved phases might be utilized for estimating expected effective thermoelectric properties of such composite materials for any distribution and relative amount of the phases. An implementation of GEM method for the IV–VI (including SnTe and GeTe), bismuth telluride (Bi_2Te_3), higher manganese silicides (HMS) and half-Heusler classes of thermoelectric materials is described in details.

Keywords: thermoelectric, GEM, multi-phase

1. Thermoelectrics

Climate changes, due to fossil fuels combustion and greenhouse gases emission, cause deep concern about environmental conservation. Another pressing issue is sustainable energy

production that is coupled with depletion of conventional energy resources. This concern might be tackled by converting the waste heat generated in internal-combustion vehicles, factories, computers, etc. into electrical energy. Converting this waste heat into electricity will reduce fossil fuel consumption and emission of pollutants. This can be achieved by direct thermoelectric (TE) converters, as was successfully demonstrated by development of various highly efficient TE material classes, including Bi_2Te_3 [1–3] for temperatures, T, of up to ~300°C, SnTe [4, 5], PbTe [6, 7] and GeTe [8–11], for temperatures range $300 \leq T \leq 500$°C, and higher manganese silicides (HMS) [12–14], half-Heuslers [15–20], which are capable to operate at higher temperatures. Such materials require unique combination of electronic (i.e. Seebeck coefficient, α, electrical resistivity, ρ, and electronic thermal conductivity, κ_e) and lattice (i.e. lattice thermal conductivity, κ_l) properties, enabling the highest possible TE figure of merit, $ZT = \alpha^2 T/[\rho(\kappa_e + \kappa_l)]$, values, for achieving significant heat to electricity conversion efficiencies. Due to the fact, that electronic TE properties are strongly correlated, and follow opposite trends upon modifying charge carriers' concentration, many of recently developed TE materials, were focused on nano-structuring methods, capable of κ_l reduction due to lattice modifications and correspondingly increasing ZT. Such methods included alloying (for PbTe, as an example, alloying with SrTe [21, 22], MgTe [23] and CdTe [24], resulted in strained endotaxial nano-structures), applying layered structures with increased interfaces population (e.g. SnSe [25]), and thermodynamically driven phase separation reactions, generating nano-scale modulations (e.g. $Ge_xPb_{1-x}Te$ [26–28] and $Ge_x(Sn_yPb_{1-y})_{1-x}Te$ [29, 30]). All of these approaches resulted in significant increase of ZT up to ~2.5 [25] due to effective scattering of phonons by associated generated nano-features. Nevertheless, although significant enhancement of TE properties was reported due to phonon scattering by nano-structured phases in such multi-phase TE materials, most of these researches did not investigate individual electronic contributions of each of the involved phases on effective TE transport properties.

2. Multi-phase thermoelectric materials

In the last few decades, major trend is to move from pristine single-crystal TE compositions towards polycrystalline multi-phase materials. One of the reasons for that is improved shear mechanical strength of polycrystalline materials compared to single crystals, exhibiting high compression, but very low transverse strengths, required to withstand high thermal and mechanical gradients applied in practical applications. Another reason is the possibility of phonon scattering by the involved interfaces as mentioned above. Most of the TE materials investigated these days are being synthesized by powder metallurgy approach under high uniaxial mechanical pressures, deforming involved grains and phases into anisotropic geometrical morphologies, which affect the electronic transport properties. Besides, a certain amount of porosity (as a second phase) is in many cases unavoidable, adversely affecting TE transport properties. Furthermore, many of currently employed TE materials (e.g. Bi_2Te_3 and HMS) are crystallographic anisotropic with optimal TE transport properties along preferred orientations. Some researches of such materials for TE applications do not consider crystallographic anisotropy, while assuming, that randomly oriented grains of different crystallo-

http://dx.doi.org/10.5772/65099

graphic planes cancel each other in polycrystalline samples. Yet, some anisotropy can exist also in such materials in case of highly anisotropic specific properties (e.g. mechanical properties), leading to textured polycrystal. For example, texture development of non-cubic polycrystalline alloys was attributed to multiple deformation modes applied in each grain, twinning resulting in grain reorientation and strong directional grain interactions [12]. Specifically, in Bi_2Te_3, for example, exhibiting highly anisotropic layered crystal structure consists of 15 parallel layers stacked along crystallographic *c* axis, the presence of van der Waals gap in the crystal lattice, divides crystal into blocks of five mono-atomic sheets [1]. In this case, retaining the crystallographic anisotropy is highly desired. This is due to the fact, that in transverse to crystallographic *c* axis, TE power factor (numerator in *ZT* expression) is considerably higher, than in parallel to this direction, mainly due to higher electrical conductivity values. For powder metallurgy synthesized Bi_2Te_3-based materials, it was shown that moderate powder grinding pressures, might retain some of the crystallographic anisotropy, due to the weaker van der Waals bonding of atoms located in adjacent layers along *c*-axis, compared to ionic/covalent bonding between atoms located in each of the layers [31]. In this example, higher *ZT* values in transverse to powder pressing direction are expected as in single crystals. This example highlights the significance of controlling phases' morphology for optimizing TE transport properties.

Besides of metallurgical phases, individual transport properties of two species (e.g. light and heavy holes in *p*-type PbTe [32]), in materials with complicated electronic band structures might contribute dramatically to effective TE transport properties.

In this chapter, effective TE properties (Seebeck coefficient, α electrical resistivity, ρ or conductivity, $\sigma = \rho^{-1}$ and thermal conductivity, κ) of general complex structure, consisting of at least two independent phases with any respective relative amount and geometrical alignment are derived by using the GEM method [4] and individual TE properties of each of the involved phases. This approach can be utilized for maximizing TE figure of merit of multi-phase composite materials, for example, by intentional alignment of the involved phases along the optimal TE direction.

We consider in this chapter a simple formulation for modelling of multi-phase TE materials, originated from materials science aspects, such as inter-diffusion, alloying, dissolution, phase transitions, phase separation, phase segregation, precipitation, recrystallization and other phenomena, that can take place in operation conditions of TE modules, especially TE power generation modules exposed to high thermo-mechanical stresses.

3. TE GEM effective equations for two-phase materials

Effective TE properties of two-phase composites can be accurately predicted by GEM method, Eqs. (1)–(3) [4, 33–35]:

$$\frac{\alpha_{\text{eff}}-\alpha_2}{\alpha_1-\alpha_2}=\frac{\dfrac{\kappa_{\text{eff}}/\kappa_2}{\sigma_{\text{eff}}/\sigma_2}-1}{\dfrac{\kappa_1/\kappa_2}{\sigma_1/\sigma_2}-1}, \tag{1}$$

$$x_1\frac{\left(\sigma_1\right)^{1/t}-\left(\sigma_{\text{eff}}\right)^{1/t}}{\left(\sigma_1\right)^{1/t}+A\left(\sigma_{\text{eff}}\right)^{1/t}}=\left(1-x_1\right)\frac{\left(\sigma_{\text{eff}}\right)^{1/t}-\left(\sigma_2\right)^{1/t}}{\left(\sigma_2\right)^{1/t}+A\left(\sigma_{\text{eff}}\right)^{1/t}}, \tag{2}$$

$$x_1\frac{\left(\kappa_1\right)^{1/t}-\left(\kappa_{\text{eff}}\right)^{1/t}}{\left(\kappa_1\right)^{1/t}+A\left(\kappa_{\text{eff}}\right)^{1/t}}=\left(1-x_1\right)\frac{\left(\kappa_{\text{eff}}\right)^{1/t}-\left(\kappa_2\right)^{1/t}}{\left(\kappa_2\right)^{1/t}+A\left(\kappa_{\text{eff}}\right)^{1/t}}. \tag{3}$$

These three GEM equations, Eqs. (1)–(3), are usually employed for calculating effective Seebeck coefficient (α_{eff}) and effective electrical and thermal conductivities (σ_{eff} and κ_{eff}, respectively) for two-phase materials using individual electrical (σ_1 and σ_2) and thermal (κ_1 and κ_2) conductivity, as well as, individual Seebeck coefficient (α_1 and α_2) values of involved phases. Morphological parameters A, t can be derived by modelling of experimental results or from percolation equation [33, 34]. Parameter x_1 is volume fraction of one of the phases. Values of A and t are strongly affected by phase distribution and morphology. It was shown, that for homogeneously distributed second phase in continuous matrix, t value is equal to 1 [4] and the entire morphological alignment possibilities of the second phase related to the matrix phase are bounded by the so-called 'parallel' and 'series' alignment of the phases (relative to electrical potential or temperature gradients). Parameter A varies from 8 for parallel to 0 for series alignments. It can be seen, that for substituting $t = 1$ and $A = 8$ in Eqs. (2) and (3), as in the case of phases distribution in parallel to electrical current direction, reduces equations to Eq. (4), while substituting of Eq. (4) in Eq. (1) leads to Eq. (5):

$$\left(\sigma_{\text{eff}},\kappa_{\text{eff}}\right)=\left(\sigma_1,\kappa_1\right)x_1+\left(\sigma_2,\kappa_2\right)\left(1-x_1\right), \tag{4}$$

$$\alpha_{\text{eff}}=\frac{\alpha_1\sigma_1x_1+\alpha_2\sigma_2\left(1-x_1\right)}{\sigma_1x_1+\sigma_2\left(1-x_1\right)}. \tag{5}$$

Similarly, substituting $t = 1$ and $A = 0$ in Eqs. (2) and (3), as in the case of series alignment as explained above, reduces them into Eq. (6):

http://dx.doi.org/10.5772/65099

$$\left(\sigma_{\text{eff}},\kappa_{\text{eff}}\right)=\frac{\left(\sigma_1,\kappa_1\right)\left(\sigma_2,\kappa_2\right)}{\left(\sigma_1,\kappa_1\right)\left(1-x_1\right)+\left(\sigma_2,\kappa_2\right)x_1}. \tag{6}$$

Please note that although for the case of parallel alignment, effective electrical and thermal conductivity, Eq. (4), follow a simple rule of mixture, a more complicated dependency is apparent for series alignment, Eq. (6). Yet, as shown in Eq. (7), for this latter case, effective electrical resistivity, $\rho_{\text{eff}} = \sigma_{\text{eff}}^{-1}$, follows the rule of mixture:

$$\rho_{\text{eff}}=\rho_1 x_1+\rho_2\left(1-x_1\right). \tag{7}$$

Substituting of Eq. (6) in Eq. (1), leads in this case to Eq. (8):

$$\alpha_{\text{eff}}=\frac{\alpha_1\kappa_2 x_1+\alpha_2\kappa_1\left(1-x_1\right)}{\kappa_1\left(1-x_1\right)+\kappa_2 x_1}. \tag{8}$$

While investigating Eqs. (5) and (8) , for the cases of parallel and series alignment, respectively, it can be easily seen, that for both cases, effective Seebeck coefficient depends not only on individual Seebeck coefficients of the two phases, but also on other electronic transport properties, electrical conductivity of the involved phases for the case of parallel alignment, Eq. (5), and thermal conductivity of the involved phases for the case of series alignment, Eq. (8). An explanation for this observation is given in the next section.

4. Analytical effective equations for multi-phase materials

In order to extend GEM, Eqs. (1)–(3) listed above for two-phase composite materials, into higher-ordered composites with three or more coexisting phases, a simple analytical model for calculating effective TE properties of several conductors, subjected to external electrical and thermal gradients, can be applied. For this purpose, two boundary conditions explained above, can be examined; one for conductors connected in parallel to both thermal and electrical applied gradients and the other for conductors connected in series.

4.1. Thermoelectric phases in parallel

In the case of three distributed conductors oriented in parallel to external temperature, $\Delta T = T_h - T_c$, and electrical potentials, V, gradients, shown schematically as 1, 2 and 3 in **Figure 1(a)**, each of them might be considered as a single phase with sample's length and perspective cross-section area according to its relative amount (**Figure 1b**). For this case, electrical analogue, shown in **Figure 1(c)**, includes three parallel branches, with power source reflecting the individual open circuit voltage developed according to Seebeck effect ($V_{1,2,3} = \alpha_{1,2,3}\Delta T$, where $\alpha_{1,2,3}$ – Seebeck coefficients of the involved phases) under applied temperature difference,

connected serially to resistor $R_{1,2,3}$, reflecting internal total electrical resistance, of each of the phases. In this case, electrical currents $I_{1,2,3}$, flowing through connectors are given by Eq. (9):

$$I_{1,2,3} = \frac{V - \int_{T_c}^{T_h} \alpha_{1,2,3} dT}{R_{1,2,3}}. \tag{9}$$

Total electrical current I in three-phase system is given by Eq. (10):

$$I = I_1 + I_2 + I_3 = V\left(\frac{1}{R_1} + \frac{1}{R_2} + \frac{1}{R_3}\right) - \int_{T_c}^{T_h}\left(\frac{\alpha_1}{R_1} + \frac{\alpha_2}{R_2} + \frac{\alpha_3}{R_3}\right) dT. \tag{10}$$

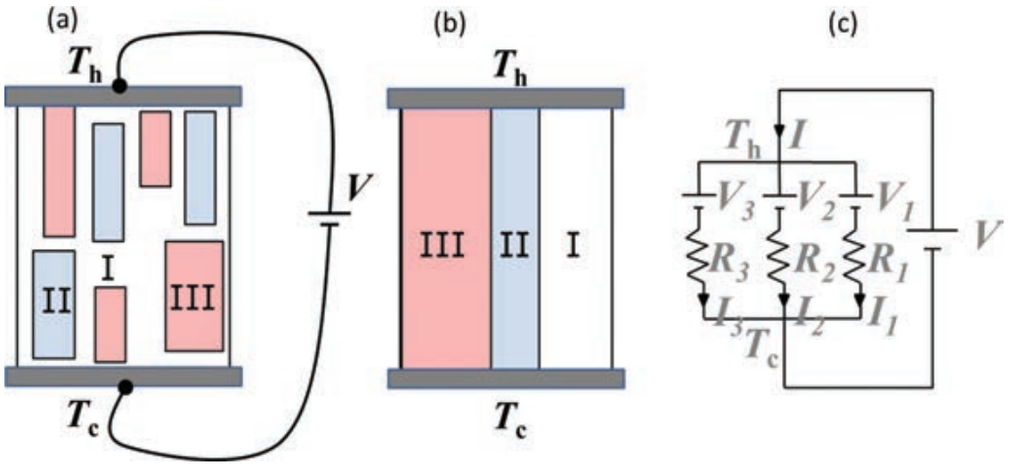

Figure 1. Schematical description of three phases, I–III, oriented in parallel to external temperature and electrical gradients, as distributed in the sample (a) and as combined entities with sample's length and perspective cross-section area according to their relative amount (b). The electrical analogue of this three-phase material is given in (c).

Considering definition of Seebeck coefficient as derivative of applied voltage with respect to temperature for non-current flowing condition, Eq. (11), a simple manipulation of Eq. (10) gives Eq. (12), which describes effective Seebeck coefficient, α_{eff}, of parallel connected three-phase structure:

$$\alpha_{eff} \overset{\text{def}}{=} \left.\frac{dV}{dT}\right|_{I=0}, \tag{11}$$

$$\alpha_{\text{eff}} = \frac{\frac{\alpha_1}{R_1} + \frac{\alpha_2}{R_2} + \frac{\alpha_3}{R_3}}{\frac{1}{R_1} + \frac{1}{R_2} + \frac{1}{R_3}} = \frac{\alpha_1 R_2 R_3 + \alpha_2 R_1 R_3 + \alpha_3 R_1 R_2}{R_2 R_3 + R_1 R_3 + R_1 R_2}. \tag{12}$$

http://dx.doi.org/10.5772/65099

Using specific parameters (resistivity $\rho_{1,2,3}$ and conductivity $\sigma_{1,2,3} = (\rho_{1,2,3})^{-1}$) instead of resistances $R_{1,2,3}$, as described in Eq. (13), expression for α_{eff} for parallel connected three-phase structures can be derived, Eq. (14):

$$R_{1,2,3} = \frac{\rho_{1,2,3} l_{\text{samp}}}{\tilde{A}_{1,2,3}}, \tag{13}$$

$$\alpha_{eff} = \frac{\left(\frac{\alpha_1\rho_2\rho_3}{\tilde{A}_2\tilde{A}_3} + \frac{\alpha_2\rho_1\rho_3}{\tilde{A}_1\tilde{A}_3} + \frac{\alpha_3\rho_1\rho_2}{\tilde{A}_1\tilde{A}_2}\right)}{\left(\frac{\rho_2\rho_3}{\tilde{A}_2\tilde{A}_3} + \frac{\rho_1\rho_3}{\tilde{A}_1\tilde{A}_3} + \frac{\rho_1\rho_2}{\tilde{A}_1\tilde{A}_2}\right)} = \frac{\alpha_1\tilde{A}_1\rho_2\rho_3 + \alpha_2\tilde{A}_2\rho_1\rho_3 + \alpha_3\tilde{A}_3\rho_1\rho_2}{\tilde{A}_1\rho_2\rho_3 + \tilde{A}_2\rho_1\rho_3 + \tilde{A}_3\rho_1\rho_2} = \frac{\alpha_1\sigma_1\tilde{A}_1 + \alpha_2\sigma_2\tilde{A}_2 + \alpha_3\sigma_3\tilde{A}_3}{\sigma_1\tilde{A}_1 + \sigma_2\tilde{A}_2 + \sigma_3\tilde{A}_3}, \tag{14}$$

where, $l_{\text{samp}} = l_1 = l_2 = l_3$ is the sample's length, $\tilde{A}_{1,2,3}$ is the cross-section area transverse to electrical current flow.

While considering, volume fractions, $x_{1,2,3}$ ($= \tilde{A}_{1,2,3} \cdot l_{\text{samp}}/V_{\text{samp}}$, where V_{samp} is sample's volume) of the respective phase, Eq. (15) can be easily derived:

$$\left(\alpha_{\text{eff}}\right)_{\text{parallel}} = \frac{\alpha_1\sigma_1 x_1 + \alpha_2\sigma_2 x_2 + \alpha_3\sigma_3 x_3}{\sigma_1 x_1 + \sigma_2 x_2 + \sigma_3 x_3} = \frac{\sum \alpha_i\sigma_i x_i}{\sum \sigma_i x_i}. \tag{15}$$

From electrical analogue shown in **Figure 1(c)**, effective electrical and thermal conductivities can also be easily derived, as expressed in Eqs. (16) and (17), respectively:

$$\left(\sigma_{\text{eff}}\right)_{\text{parallel}} = \sigma_1 x_1 + \sigma_2 x_2 + \sigma_3 x_3 = \sum \sigma_i x_i, \tag{16}$$

$$\left(\kappa_{\text{eff}}\right)_{\text{parallel}} = \kappa_1 x_1 + \kappa_2 x_2 + \kappa_3 x_3 = \sum \kappa_i x_i. \tag{17}$$

It is noteworthy that applying the same approach for higher *i*-ordered multi-phase materials will follow the general-ordered right-hand side expressions of Eqs. (15)–(17). Furthermore, it can be easily seen that Eqs. (15)–(17) for the case of two-phase materials are reduced to Eqs. (5) and (4), respectively, derived from the GEM method.

4.2. Thermoelectric phases in series

Equivalent description for the case of three distributed conductors oriented in series to external temperature and electrical potentials gradients is shown in **Figure 2(a)**.

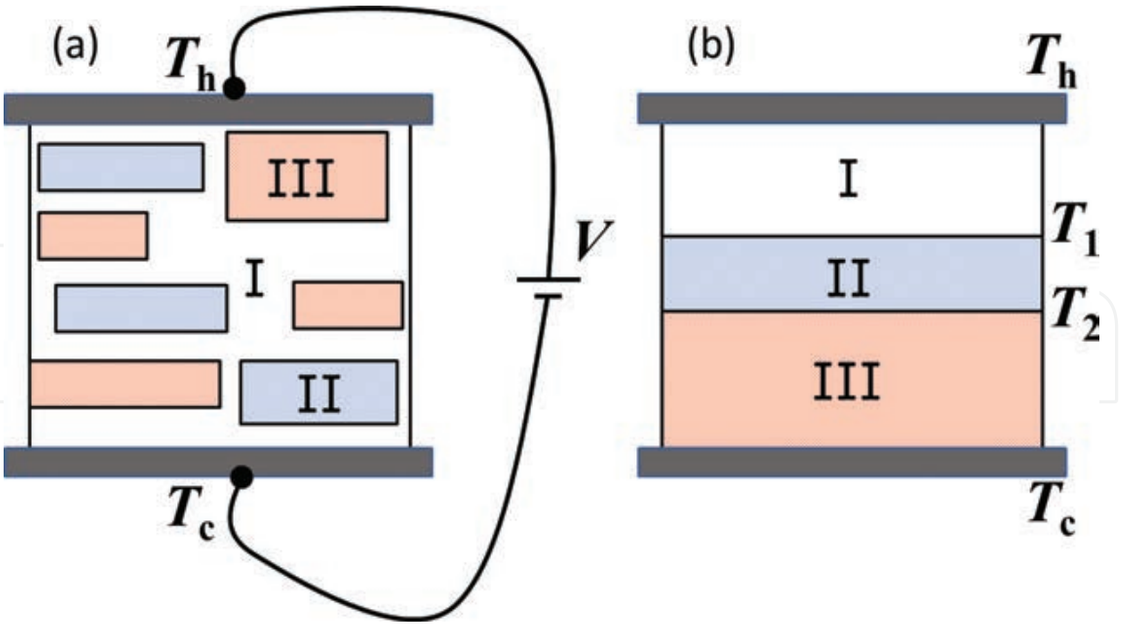

Figure 2. Schematical description of three phases, I–III, oriented in series to external temperature and electrical gradients, as distributed in the sample (a) and as combined entities with sample's diameter and perspective lengths according to their relative amount (b).

For this case, a similar analysis is presented, taking into account individual thermal gradients applied on each of the phases. Taking into account that the first, second and third phases are subjected to temperature differences of $(T_h - T_1)$, $(T_1 - T_2)$ and $(T_2 - T_c)$, respectively, as shown in **Figure 2(b)**, where $T_{1,2}$ are intermediate temperatures ($T_h > T_1 > T_2 > T_c$), effective Seebeck coefficient of such serially aligned three-phase samples can be described in terms of Eq. (18):

$$\alpha_{\text{eff}} = \frac{\alpha_1(T_h - T_1) + \alpha_2(T_1 - T_2) + \alpha_3(T_2 - T_c)}{T_h - T_c}. \tag{18}$$

Under adiabatic heat conduction conditions, where no lateral heat losses are apparent, the heat flow, Q, through the entire sample and the individual phases can be described in terms of unidirectional Fourier heat conduction equation, Eq. (19):

$$Q = \frac{\kappa_1 \tilde{A}}{l_1}(T_h - T_1) = \frac{\kappa_2 \tilde{A}}{l_2}(T_1 - T_2) = \frac{\kappa_3 \tilde{A}}{l_3}(T_2 - T_c) = \frac{\kappa_{\text{eff}} \tilde{A}}{l_{\text{samp}}}(T_h - T_c), \tag{19}$$

where κ_{eff} is effective thermal conductivity of the three-phase material, $\tilde{A}$ is cross-section area transverse to heat flow and $\kappa_{1,2,3}$ and $l_{1,2,3}$ are thermal conductivity and effective length of each of the involved phases, respectively.

Using expression (19), the numerator terms of Eq. (18) can be easily described in terms of expressions (20):

http://dx.doi.org/10.5772/65099

$$\alpha_1\left(T_h - T_1\right) = \frac{Ql_1\alpha_1}{\kappa_1\tilde{A}}, \alpha_2\left(T_1 - T_2\right) = \frac{Ql_2\alpha_2}{\kappa_2\tilde{A}}, \alpha_3\left(T_2 - T_c\right) = \frac{Ql_3\alpha_3}{\kappa_3\tilde{A}}. \tag{20}$$

In the rightmost equation of expression (19), $\kappa_{\text{eff}}\tilde{A}/l_{\text{samp}}$ represents overall thermal conductance, K_{eff} of the three-phase sample, which is described in Eq. (21), in terms of serially connected thermal resistances, $R_{\text{th},1,2,3}$, specified in Eq. (22):

$$K_{\text{eff}} = \frac{\kappa_{\text{eff}}\tilde{A}}{l_{\text{samp}}} = \frac{1}{\left(R_{\text{th}}\right)_1 + \left(R_{\text{th}}\right)_2 + \left(R_{\text{th}}\right)_3}, \tag{21}$$

$$\left(R_{\text{th}}\right)_{1,2,3} = \frac{1}{\left(\frac{\kappa_{1,2,3}\tilde{A}}{l_{1,2,3}}\right)}. \tag{22}$$

Combining Eqs. (21) and (22) leads to Eq. (23):

$$K_{\text{eff}} = \frac{1}{\frac{l_1}{\kappa_1\tilde{A}} + \frac{l_2}{\kappa_2\tilde{A}} + \frac{l_3}{\kappa_3\tilde{A}}}. \tag{23}$$

Substitution of the expression of K_{eff}, Eq. (23) in the rightmost term of expression (19) results in the expression of $T_h - T_c$, presented in Eq. (24):

$$Q = \frac{1}{\frac{l_1}{\kappa_1\tilde{A}} + \frac{l_2}{\kappa_2\tilde{A}} + \frac{l_3}{\kappa_3\tilde{A}}}\left(T_h - T_c\right) or \left(T_h - T_c\right) = Q\left(\frac{l_1}{\kappa_1\tilde{A}} + \frac{l_2}{\kappa_2\tilde{A}} + \frac{l_3}{\kappa_3\tilde{A}}\right). \tag{24}$$

Substitution of temperature differences derived in Eqs. (20) and (24) into Eq. (18) results in the expression of α_{eff} for serially connected three-phase structures, Eq. (25):

$$\left(\alpha_{eff}\right)_{series} = \frac{\left(\frac{Ql_1\alpha_1}{\kappa_1\tilde{A}} + \frac{Ql_2\alpha_2}{\kappa_2\tilde{A}} + \frac{Ql_3\alpha_3}{\kappa_3\tilde{A}}\right)}{Q\left(\frac{l_1}{\kappa_1\tilde{A}} + \frac{l_2}{\kappa_2\tilde{A}} + \frac{l_3}{\kappa_3\tilde{A}}\right)} = \frac{\left(\frac{\alpha_1 x_1}{\kappa_1} + \frac{\alpha_2 x_2}{\kappa_2} + \frac{\alpha_3 x_3}{\kappa_3}\right)}{\left(\frac{x_1}{\kappa_1} + \frac{x_2}{\kappa_2} + \frac{x_3}{\kappa_3}\right)} = \frac{\sum\frac{\alpha_i x_i}{\kappa_i}}{\sum\frac{x_i}{\kappa_i}}. \tag{25}$$

Applying the same considerations described above, effective electrical and thermal conductivities can also be derived, as expressed in Eqs. (26) and (27), respectively:

$$\left(\sigma_{\text{eff}}\right)_{\text{series}} = \frac{1}{\frac{x_1}{\sigma_1} + \frac{x_2}{\sigma_2} + \frac{x_3}{\sigma_3}} = \frac{1}{\left(\sum \frac{x_i}{\sigma_i}\right)}, \tag{26}$$

$$\left(\kappa_{\text{eff}}\right)_{\text{series}} = \frac{1}{\frac{x_1}{\kappa_1} + \frac{x_2}{\kappa_2} + \frac{x_3}{\kappa_3}} = \frac{1}{\left(\sum \frac{x_i}{\kappa_i}\right)}. \tag{27}$$

Similarly to the previous case of parallel-connected phases, *i*-ordered multi-phase materials will follow general-ordered right-hand side expressions of Eqs. (25)–(27). Furthermore, it can be easily seen, that Eq. (25) and Eqs. (26) and (27) for the case of two-phase materials are reduced to Eqs. (8) and (6), respectively, derived from the GEM method, highlighting validity of the analytic approach described here.

5. Practical examples and applications

Prior to describing the full potential of the GEM concept on optimizing performance of multi-phase TE materials, two general examples highlighting the potential of the method for monitoring the microstructure and phase morphology are described.

While analysing measured electrical and thermal conductivities of Cu following different spark plasma sintering (SPS) conditions, resulting in porosity levels in the range of 0–30%, a good agreement to GEM equations, Eqs. (2) and (3), was observed while assuming homogeneous dispersion ($t = 1$) and nearly spherical morphology ($A = 2$), as were observed by electronic microscopy, as well as σ_1, κ_1 values of pure Cu (the matrix phase), and σ_2, κ_2 equal to zero (the pores phase) [36]. This approach not just validated experimentally the GEM equations described above, but also paved a route for monitoring porosity amount during SPS consolidation process, which is widely applied in the synthesis of TE materials, as pointed out above, just by measuring electrical resistivity of the samples. For the SnTe system in the two-phase compositional range between pure Sn and SnTe compound, a parallel morphological alignment of the phases was identified both by electronic microscopy and by measuring Seebeck coefficient values of the samples [4]. The latter was validated by comparing measured α_{eff} to values, calculated by GEM equation, Eq. (1), with various A values. The best agreement was obtained for $A = 8$, indicating a parallel alignment of the phases. This approach validated the possibility to identify geometrical alignment of the phases just by measuring Seebeck coefficient values without any requirement of advanced electron microscopy.

Specifically, for TE materials, it was recently shown that upon introduction of $MoSe_2$ phase into layered *n*-type $Bi_2Te_{2.4}Se_{0.6}$ alloy for optimizing its TE performance, the best performance was obtained for oriented samples with $A = 0.3$, in Eqs. (1)–(3), as shown, for example, for ρ_{eff}, in **Figure 3(a)** [3]. In this figure, the agreement of red experimental points with $A = 0.3$ curve can be clearly seen.

http://dx.doi.org/10.5772/65099

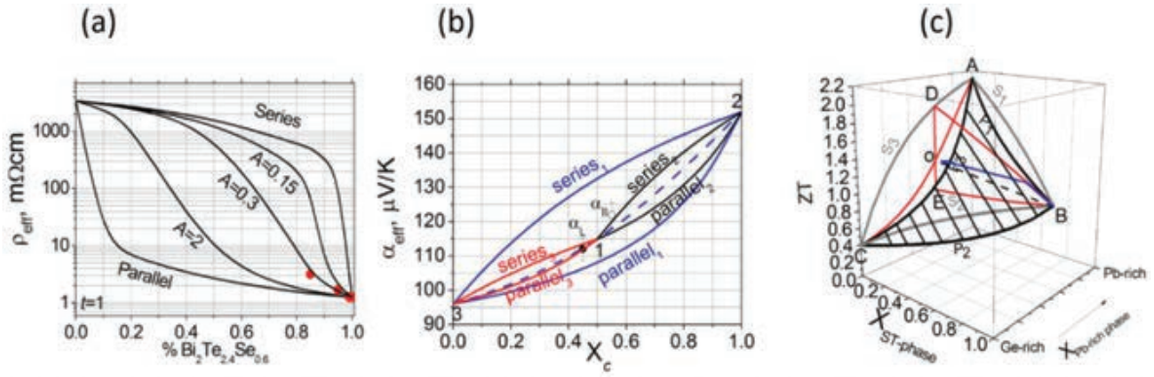

Figure 3. (a) Variations of effective electrical resistivity values upon introduction of $MoSe_2$ in $Bi_2Te_{2.4}Se_{0.6}$-$MoSe_2$ two-phase system [3]. (b) Room temperature GEM analysis of effective Seebeck coefficient upon homogeneous mixing (t = 1) of c-axis and a-axis oriented grains of HMS for different geometrical alignment (0,*series*<A<∞,*parallel*) conditions [12]. (c) Interaction of ZT surfaces and volumes between three phases, solution treated (ST) matrix (B), Pb-rich (A) and Ge-rich (C) phases of $Pb_{0.25}Sn_{0.25}Ge_{0.5}Te$. The entire interaction volumes are bounded by ABC points, where each volume is bounded by two surfaces of series (S_1-S_2-S_3) and parallel (P_1-P_2-P_3) alignments [37].

A similar approach was recently applied for investigation of the morphological effects on TE properties of $Ti_{0.3}Zr_{0.35}Hf_{0.35}Ni_{1+\delta}Sn$ alloys following phase separation into half-Heulser $Ti_{0.3}Zr_{0.35}Hf_{0.35}NiSn$ and Heusler $Ti_{0.3}Zr_{0.35}Hf_{0.35}Ni_2Sn$ phases [15]. In this research, it was found that although phases' orientation was aligned in intermediate level (A = 0.8) between parallel (A = 8) and spherical (A = 2) alignments, enhanced TE performance is expected in a series alignment while substituting A=0 in Eqs. (1)–(3).

Another very interesting implementation of GEM approach was recently applied to estimate effective room temperature Seebeck coefficient and electrical resistivity values of a randomly morphological oriented homogeneous mixture of (001) and (hk0) grains in anisotropic polycrystalline HMS TE samples [12]. Applying GEM analysis to homogeneous distribution of (001) and (hk0) oriented grains (t = 1), for different alignment (A) conditions, resulted in the blue curves shown in **Figure 3(b)**. In this figure, the upper and lower blue curves represent series and parallel alignments of two configurations, respectively, points 2 and 3 represent c- and a-axis-oriented crystals, respectively, and intermediate dashed blue curve indicates a spherical distribution of two directions. Point 1 indicates 50% mixture of the directions for a spherical alignment, representing mixture of two directions, as in the case of non-textured polycrystalline HMS powder. The black and red curves of **Figure 3(b)** indicate interaction between c- and a-axis-oriented grains with randomly distributed polycrystalline powder (point 1 in **Figure 3b**), as was calculated by GEM approach. In that case, a partial c-axis preferred orientated powder, embedded in a homogeneous surrounding of macroscopic non-preferred-orientated powder is expected to exhibit α_{eff} values that are bounded in between the $series_2$ and $parallel_2$ black curves of the figures. Similarly, α_{eff} values for partial a-axis preferred orientated powder are expected to be bounded between $series_3$ and $parallel_3$ red curves of the figure. The experimentally measured $\alpha_{\parallel}$, $\alpha_{\perp}$ values while considering 10% preferred orientation, as was identified by XRD, are also shown in the figure. It can be seen that experimental points lie in the interaction zone between c- and a-axis-orientated powder and a randomly distributed powder, bounded by the black and red curves, respectively. This indicates the

validity of proposed calculation route to estimate electronic transport properties of textured polycrystalline materials. It can be also seen that for HMS, ~10% preferred orientation of both of investigated directions is almost independent of the orientation of the grains, and, therefore, controlling the alignment of the grains morphology is not expected to affect the effective Seebeck coefficient.

Implementation of GEM concept in three-phase TE materials, based on Eqs. (15)–(17) and (25)–(27), was recently shown for quasi-ternary GeTe-PbTe-SnTe system [37, 38]. Specifically, it was shown that phase separation of solution-treated (ST) $Pb_{0.25}Sn_{0.25}Ge_{0.5}Te$ composition (phase B in **Figure 3c**) into Pb-rich, $Pb_{0.33}Sn_{0.3}Ge_{0.37}Te$ (phase A), and Ge-rich, $Pb_{0.1}Sn_{0.17}Ge_{0.73}Te$ (phase C) phases is apparent in the system. In this system, prolonged thermal treatments at each temperature resulted, at the first stages, in three phases, parent B phase and two decomposed A and C phases. This stage is terminated by full decomposition into A and C, where only these phases are apparent. Furthermore, a lamellar alignment of the phases was observed at the first 24 h of thermal treatment, while prolonged treatments were resulted in spheroidization, due to reduced surface area free energy at this configuration. It was also observed that ZT values were increased during the first 24 h while reduced at more prolonged durations. For explaining these experimental evidences, GEM approach was applied, as shown in **Figure 3(c)**. In this figure, triangle BDE indicates the specific interaction surface for separation of the phase B into the phases A and C, where BD side of triangle represents series ('lamellar') alignment morphology and BE represents parallel alignment of the phases. The dashed BO line represents spherical alignment. It can be easily shown that measured ZT values, indicated by the blue line, indeed follow the series alignment (BD line) at the first decomposition stages, but from this point on approach the dashed BO line until a full spheroidization is occurred (at point o). From this analysis, it was concluded that any theoretical possibility for retaining the lamellar morphology in this system would result in even higher ZT values of up to ~1.8 after a complete decomposition of the matrix into the two involved separation phases.

6. Concluding remarks

In this chapter, the potential of GEM approach to optimize electronic properties of multi-phase thermoelectric materials in terms of compositional or morphological considerations is shown in details. This approach already proved itself in monitoring of the densification rate of powder metallurgy processed materials, as well as in the determination of compositional modifications in binary systems just by measuring one of the transport properties. It is just beginning to approach the true potential to optimize thermoelectric transport properties of multi-phase materials, such as those containing embedded nano-features for reduction of the lattice thermal conductivity, where electronic contribution of the involved phase is usually neglected. It was shown that method does not just explain unexpected electronic trends in such materials, but might be employed for prediction of synthesis routes for optimizing thermoelectric figure of merit based on different compositions or alignment morphologies.

Based on the pointed above examples, it is obvious that for TE power generators operating at low (<300°C), intermediate (300–500°C) and high (>500°C) temperature ranges, Bi_2Te_3, PbTe/

http://dx.doi.org/10.5772/65099

GeTe and HMS/half-Heusler-based compositions might be employed. In such systems, identifying compositions enabling phase separation or precipitation into multi-phases, according to specific phase diagram, has a potential to reduce lattice thermal conductivity. Yet, for maximizing TE potential, optimal geometrical alignment of the phases should be identified. Using the proposed approach, based on individual TE transport properties of the involved phases, optimal geometrical alignment direction might be identified, leading to enhanced TE performance, enabling a real contribution to the society by reducing our dependence on fossil fuels and by minimizing emission of greenhouse gases.

Acknowledgements

The work was supported by the Ministry of National Infrastructures, Energy and Water Resources grant (3/15), No. 215-11-050.

Author details

Yaniv Gelbstein

Address all correspondence to: yanivge@bgu.ac.il

Department of Materials Engineering, Ben-Gurion University of the Negev, Beer-Sheva, Israel

References

[1] Meroz O, Ben-Ayoun D, Beeri O, Gelbstein Y. Development of $Bi_2Te_{2.4}Se_{0.6}$ Alloy for thermoelectric power generation applications. Journal of Alloys and Compounds. 2016; 679:196–201.

[2] Vizel R, Bargig T, Beeri O, Gelbstein Y. Bonding of Bi_2Te_3 based thermoelectric legs to metallic contacts using $Bi_{0.82}Sb_{0.18}$ alloy. Journal of Electronic Materials. 2016; 45(3):1296–1300.

[3] Shalev T, Meroz O, Beeri O, Gelbstein Y. Investigation of the influence of $MoSe_2$ on the thermoelectric properties of n-type $Bi_2Te_{2.4}Se_{0.6}$. Journal of Electronic Materials. 2015; 44(6):1402.

[4] Gelbstein Y. Thermoelectric power and structural properties in two phase Sn/SnTe Alloys. Journal of Applied Physics. 2009; 105:023713.

[5] Guttmann GM, Dadon D, Gelbstein Y. Electronic tuning of the transport properties of off-stoichiometric $Pb_xSn_{1-x}Te$ thermoelectric alloys by Bi_2Te_3 doping. Journal of Applied Physics. 2015; 118:065102.

[6] Cohen I, Kaller M, Komisarchik G, Fuks D, Gelbstein Y. Enhancement of the thermoelectric properties of *n*-type PbTe by Na and Cl co-doping. Journal of Materials Chemistry C. 2015; 3:9559–9564.

[7] Gelbstein Y, Dashevsky Z, Dariel MP. In-doped $Pb_{0.5}Sn_{0.5}Te$ *p*-type samples prepared by powder metallurgical processing for thermoelectric applications. Physica B. 2007; 396:16–21.

[8] Hazan E, Ben-Yehuda O, Madar N, Gelbstein Y. Functional graded germanium-lead chalcogenides-based thermoelectric module for renewable energy applications. Advanced Energy Materials. 2015; 5(11):1500272.

[9] Hazan E, Madar N, Parag M, Casian V, Ben-Yehuda O, Gelbstein Y. Effective electronic mechanisms for optimizing the thermoelectric properties of GeTe rich alloys. Advanced Electronic Materials. 2015; 1:1500228.

[10] Gelbstein Y, Davidow J. Highly-efficient functional $Ge_xPb_{1-x}Te$ based thermoelectric alloys. Physical Chemistry and Chemical Physics. 2014; 16:20120.

[11] Davidow J, Gelbstein Y. A comparison between the mechanical and thermoelectric properties of the highly efficient *p*-type GeTe rich compositions – TAGS-80, TAGS-85 and 3 % Bi_2Te_3 doped $Ge_{0.87}Pb_{0.13}Te$. Journal of Electronic Materials. 2013; 42(7):1542–1549.

[12] Sadia Y, Aminov Z, Mogilyansky D, Gelbstein Y. Texture anisotropy of higher manganese silicide following arc-melting and hot-pressing. Intermetallics. 2016; 68:71–77.

[13] Sadia Y, Madar N, Kaler I, Gelbstein Y. Thermoelectric properties in the quasi-binary $MnSi_{1.73}$-$FeSi_2$ system. Journal of Electronic Materials. 2015; 44(6):1637.

[14] Sadia Y, Elegrably M, Ben-Nun O, Marciano Y, Gelbstein Y. Sub-micron features in higher manganese silicide. Journal of Nanomaterials. 2013; 701268.

[15] Appel O, Zilber T, Kalabukhov S, Beeri O, Gelbstein Y. Morphological effects on the thermoelectric properties of $Ti_{0.3}Zr_{0.35}Hf_{0.35}Ni_{1+\delta}Sn$ alloys following phase separation. Journal of Materials Chemistry C. 2015; 3:11653–11659.

[16] Kirievsky K, Sclimovich M, Fuks D, Gelbstein Y. *Ab initio* study of the thermoelectric enhancement potential in nano grained TiNiSn. Physical Chemistry and Chemical Physics. 2014; 16:20023.

[17] Appel O, Gelbstein Y. A comparison between the effects of Sb and Bi doping on the thermoelectric properties of the $Ti_{0.3}Zr_{0.35}Hf_{0.35}NiSn$ half-Heusler alloy. Journal of Electronic Materials. 2014; 43(6):1976–1982.

[18] Kirievsky K, Gelbstein Y, Fuks D. Phase separation and antisite defects possibilities for enhancement the thermoelectric efficiency in TiNiSn half-Heusler alloys. Journal of Solid State Chemistry. 2013; 203:247–254.

[19] Appel O, Schwall M, Kohne M, Balke B, Gelbstein Y. Microstructural evolution effects of spark plasma sintered $Ti_{0.3}Zr_{0.35}Hf_{0.35}NiSn$ half-Heusler compound on the thermoelectric properties. Journal of Electronic Materials. 2013; 42(7):1340–1345.

[20] Gelbstein Y, Tal N, Yarmek A, Rosenberg Y, Dariel MP, Ouardi S, Balke B, Felser C, Köhne MM. Thermoelectric properties of spark plasma sintered composites based on TiNiSn half Heusler alloys. Journal of Materials Research. 2011; 26(15):1919–1924.

[21] Biswas K, He J, Blum ID, Chun-I-Wu, Hogan TP, Seidman DN, Dravid VP, Kanatzidis M. High-performance bulk thermoelectrics with all-scale hierarchial architectures. Nature. 2012; 489:414.

[22] Biswas K, He J, Zhang Q, Wang G, Uher C, Dravid VP, Kanatzidis MG. Strained endotaxial nanostructures with high thermoelectric figure of merit. Nature Chemistry. 2011; 3:160.

[23] Ohta M, Biswas K, Lo S-H, He J, Chung DY, Dravid VP, Kanatazidis MG. Enhancement of thermoelectric figure of merit by the insertion of MgTe nanostructures in *p*-type PbTe doped with Na_2Te. Advanced Energy Materials. 2012; 2:1117–1123.

[24] Pei Y, LaLonde AD, Heinz NA, Snyder GJ. High thermoelectric figure of merit in PbTe alloys demonstrated in PbTe-CdTe. Advanced Energy Materials. 2012; 2:670–675.

[25] Zhao L-D, Lo S-H, Zhang Y, Sun H, Tan G, Uher C, Wolverton C, Dravid VP, Kanatzidis MG. Ultralow thermal conductivity and high thermoelectric figure of merit in SnSe crystals. Nature. 2014; 508:373.

[26] Gelbstein Y, Davidow J, Girard SN, Chung DY, Kanatzidis M. Controlling metallurgical phase separation reactions of the $Ge_{0.87}Pb_{0.13}Te$ alloy for high thermoelectric performance. Advanced Energy Materials. 2013; 3:815–820.

[27] Gelbstein Y, Dashevsky Z, Dariel MP. Highly efficient bismuth telluride doped *p*-type $Pb_{0.13}Ge_{0.87}Te$ for thermoelectric applications. Physica Status Solidi (RRL). 2007; 1(6): 232–234.

[28] Gelbstein Y, Dado B, Ben-Yehuda O, Sadia Y, Dashevsky Z, Dariel MP. Highly efficient Ge-rich $Ge_xPb_{1-x}Te$ thermoelectric alloys. Journal of Electronic Materials. 2010; 39(9): 2049.

[29] Gelbstein Y, Rosenberg Y, Sadia Y, Dariel MP. Thermoelectric properties evolution of spark plasma sintered $(Ge_{0.6}Pb_{0.3}Sn_{0.1})Te$ following a spinodal decomposition. Journal of Physical Chemistry C. 2010; 114:13126–13131.

[30] Rosenberg Y, Gelbstein Y, Dariel MP. Phase separation and thermoelectric properties of the $Pb_{0.25}Sn_{0.25}Ge_{0.5}Te$ compound. Journal of Alloys and Compounds. 2012; 526:31–38.

[31] Ben-Yehuda O, Gelbstein Y, Dashevsky Z, Shuker R, Dariel MP. Highly textured Bi_2Te_3-based materials for thermoelectric energy conversion. Journal of Applied Physics. 2007; 101:113707.

[32] Gelbstein Y, Dashevsky Z, Dariel MP. The search for mechanically stable PbTe based thermoelectric materials. Journal of Applied Physics. 2008; 104:033702.

[33] Webman I, Jortner J, Cohen MH. Thermoelectric power in inhomogeneous materials. Physical Review B. 1977; 16(6):2959–2964.

[34] Bergman DJ, Levy O. Thermoelectric properties of a composite medium. Journal of Applied Physics. 1991; 70:6821.

[35] McLachlan DS, Blaszkiwicz M, Newnham RE. Electrical resistivity of composites. Journal of American Ceramic Society. 1990; 73(8):2187–2203.

[36] Gelbstein Y, Haim Y, Kalabukhov S, Kasiyan V, Hartman S, Rothe S, Frage N. Correlation between thermal and electrical properties of spark plasma sintered (SPS) porous copper. In: Lakshmanan A, editor. Sintering, InTech Publisher, Rijeka, Croatia. 2014. ISBN 978-953-51-4113-6

[37] Gelbstein Y. Phase morphology effects on the thermoelectric properties of $Pb_{0.25}Sn_{0.25}Ge_{0.5}Te$. Acta Materialia. 2013; 61(5):1499–1507.

[38] Gelbstein Y. Morphological effects on the electronic transport properties of three-phase thermoelectric materials. Journal of Applied Physics . 2012; 112:113721.